ISSN 0469-4732

INSTITUTE OF PLASMA PHYSICS

NAGOYA UNIVERSITY

Experimental Study on the Deposition Profile of the ICRF Power and Electron Thermal Diffusivity

Y. Ogawa, R. Ando, E. Kako, K. Kawahata, Y. Kawasumi, S. Morita, T. Watari, R. Akiyama, Y. Hamada, S. Hirokura, K. Masai, K. Matsuoka, A. Mohri, N. Noda, I. Ogawa, K. Ohkubo, K. Sato, S. Tanahashi, Y. Taniguchi, K. Toi

(Received — Apr. 10, 1989)

IPPJ- 908 Apr. 1989

RESEARCH REPORT

NAGOYA, JAPAN

Experimental Study on the Deposition Profile of the ICRF Power and Electron Thermal Diffusivity

Y. Ogawa, R. Ando, E. Kako[a)], K. Kawahata, Y. Kawasumi, S. Morita, T. Watari, R. Akiyama, Y. Hamada, S. Hirokura, K. Masai, K. Matsuoka, A. Mohri, N. Noda, I. Ogawa, K. Ohkubo, K. Sato, S. Tanahashi, Y. Taniguchi, K. Toi,

Inst. of Plasma Physics, Nagoya Univ., Nagoya 464-01, Japan

(Received - April 10, 1989)
IPPJ-908 April 1989

Further communication about this report is to be sent to the Research Information Center, Institute of Plasma Physics, Nagoya University, Nagoya, 464-01, Japan.

Abstract

In ICRF heating experiments the deposition profile in electrons has been derived experimentally, and comparison with theory has been performed. It is found that the deposition profile is relatively broad ($P_{rfe}(r) = P_{rfe}(0)(1-(r/a)^2)^k$ with $k = 1.8$), and this is interpreted in terms of characteristics of the mode-converted Ion Bernstein Wave. The distribution of the rf power to each species (electrons, hydrogen and deuterium ions) is in good agreement with theoretical predictions. With the deposition profile experimentally obtained, the electron thermal diffusivity χ_e has been calculated, resulting in $\chi_e \sim 0.65\ m^2/s$ at $\bar{n}_e = 9\times10^{19}\ m^{-3}$.

I. Introduction

In fusion research it is one of key issues to clarify properties of thermal transport in auxiliarily heated plasmas. It is well known that thermal transport is generally anomalous, especially for electrons, and elaborated efforts have been paid to study anomalous electron transport from theoretical and experimental viewpoints.

Experimentally, if we will determine diffusion coefficients of thermal transport, it is necessary to evaluate a deposition profile of auxiliary heating power, in addition to measure profiles of plasma parameters. In Neutral Beam Injection (NBI) heating experiments, the theory for the beam deposition profile has been well established [1,2], and elaborate computer codes have already been developed to study the thermal transport for electrons (χ_e) and ions (χ_i) [3]. In Electron Cyclotron Heating (ECH) experiments, the deposition profile can also be provided by the ray-tracing code with a good validity [4].

With regard to Ion Cyclotron Range of Frequencies (ICRF) heating experiments, many theoretical efforts have been spent over several years to predict the deposition profile of the rf power to each species, by using a technique of the ray-tracing [5], or by solving a stationary wave equation as a boundary-value problem [6-10]. However we think that further work will be necessary to employ these computer codes for data analysis on the thermal transport in ICRF-heated plasmas.

On the other hand, experimentally it is also possible to determine the deposition profile of the rf power by analysing the transient phenomenon of plasmas with some assumptions. In JET experiments, the power deposition profile has been obtained from the increasing rate of the electron temperature just after the sawteeth crash [11,12]. However, it is difficult in this method to eliminate the ohmic power contribution to the sawteeth activity, and to evaluate the deposition profile outside the $q = 1$ surface.

Another method is to analyze the time behaviors of the plasma parameters just after the switch-on or switch-off of the rf pulse. With this technique, we have experimentally evaluated the rf power coupled with electrons at the whole region of the plasma column, and compared with theoretical predictions. The temporal evolutions of the electron temperature profile have been measured with a good accuracy, and the deposition profile to electrons has been derived in Section II. Comparison with theoretical results is performed in Section III. With the deposition profile experimentally obtained, the electron thermal diffusivity χ_e is estimated for ICRF-heated plasmas in Section IV. Conclusions are given in Section V.

II. Experimental study on the deposition profile

In the JIPP T-IIU tokamak (R_{maj} = 0.91 m/a = 0.23 m and B_T = 3 T), six loop antennas are installed at the high field side, and ICRF heating experiments with a power of P_{rf} = 2 MW have been conducted [13,14]. The frequency of the ICRF wave is 40 MHz and deuterium plasmas with 10 % hydrogen minority are employed, being expected the mode-conversion heating scenario.

The electron temperature profile is measured with a 10-channel grating polychromator for Electron Cyclotron Emission (ECE) measurement, where the spatial spacing of each channel is $\Delta r \sim 4$ cm (i.e., $\Delta r/a \sim 0.17$), and the data sampling time is Δt = 200 μsec [15]. The central ion temperature is measured with a fast neutral particle analyzer (FNA) of $E//B$ mass-separation type and with a crystal spectrometer ($TiXXI$ w 2.61 Å) [16]. FNA data also give informations of high energy component for hydrogen ions, which is usually observed in ICRF heating experiments. The radiation loss is measured with bolometers (metal and pyro detectors are used.) [17].

Figure 1 shows the time evolution of the electron

temperature, where the discharge with a relatively low rf power (P_{rf} = 0.9 MW) is adopted to avoid the large sawteeth activity. The rf power delivered to electrons has been calculated at the time of the switch-off, by evaluating the discontinuity of the time derivative as follows;

$$P_{rf,e}(r) = \frac{\partial W_{P,e}(r)}{\partial t}\Big|t=t_0 - \frac{\partial W_{P,e}(r)}{\partial t}\Big|t=t_1 \qquad (1)$$

where $W_{P,e} = 3/2 n_e(r) T_e(r)$, and t_0 and t_1 are the times just before and after the switch-off of the rf pulse, respectively. The time interval employed in the calculation of the time derivative in eq.(1) is much shorter (Δt < 5 ms) than the energy confinement time ($\tau_E \sim 20$ ms). It is also assumed that the electron transport coefficients (i.e., χ_e and D) does not change so rapidly during this time interval. The time derivative in eq.(1) consists of two parts; $\partial W_{P,e}/\partial t = 3/2 n_e \partial T_e/\partial t + 3/2 T_e \partial n_e/\partial t$. The first term of the right hand side is much larger than the second one, because the decay time of the density is longer than that of the electron temperature. In Fig. 2, the rf power coupled to electrons is shown, and these data are fitted to the form of

$$P_{rf,e}(r) = P_{rf,e}(0)(1 - (r/a)^2)^k \quad , \qquad (2)$$

where $P_{rf,e}(0) = 1.57$ MW/m^3 and $k = 1.8$. The deposition profile in electrons seems to be relatively broader than that measured in JET [11,12]. In addition, the amplitude of sawteeth in JIPP T-IIU is not so large ($\Delta T_{p\text{-}p}/T \sim 20$ %) compared with that in JET and PLT ($\Delta T_{p\text{-}p}/T \sim 40$–$50$ %) [18,19]. With the deposition profile experimentally obtained, the rf power deposited inside q = 1 surface is calculated to be about 20 ~ 30 % in JIPP T-IIU, and to be about 50 ~ 80 % in JET and PLT. These phenomena are explained in terms of the difference of the heating scheme; in JIPP T-IIU the electron Landau damping of the mode-converted

IBW plays a key role, and in JET and PLT the cyclotron damping of the fast wave does.

We briefly discuss the validity of eq.(1), to derive the rf power coupled with electrons. Effects of the high energy ion tail and the movement of the plasma column are taken into account. The high energy component of hydrogen ions is produced by the selective heating of the ICRF wave. After the switch-off of the rf pulse, the high energy tail is remaining and heating electrons during a relaxation time, resulting in making the decay of the electron temperature longer. The effective tail temperature is $T_{H,tail} \sim 3 \sim 4\ keV$ with $n_{H,tail}/n_{H,bulk} \sim 10 \sim 20$ % at $P_{rf} = 1\ MW$. This additional heating power is evaluated with $P_{e,tail} = 3/2\ n_e(T_{H,tail} - T_e)/\tau_{e,tail}$, resulting in $P_{e,tail} \sim 0.15\ MW/m^3$ around the cyclotron resonance layer.

Next, let us evaluate a virtual deposition power caused by the movement of the plasma column. Just after the switch-off of the rf pulse, the plasma column moves inward slightly due to the decrease of beta poloidal value, and settles at a fixed position by the feedback control. The movement of the plasma column in the horizontal direction induces some change in electron temperatures determined with ECE measurement, because the electron cyclotron emission is strongly correlated with the major radius, not with a minor radius of the plasma column. In ICRF-heated plasmas with $P_{rf} = 1\ MW$, the movement of the plasma column is $\Delta_{move} \sim 1.0\ cm$ with a time of $\tau_{move} \sim 6\ msec$. We can calculate the virtual deposition power due to the movement of the plasma column with the equation of $P_{e,move} = 3/2 n_e \Delta T_{e,move}/\tau_{move}$, where $\Delta T_{e,move} = T_e(r+\Delta_{move}) - T_e(r)$. This virtual power is negligibly small at the plasma center ($P_{e,move}(r=0) \sim 0.04\ MW/m^3$), but becomes large at the region of $r/a \sim 0.3$ ($P_{e,move}(r/a=0.3) \sim 0.35\ MW/m^3$).

These virtual deposition powers, $P_{e,tail}$ and $P_{e,move}$, caused by the high energy tail and the movement of the plasma column are plotted in Fig. 2. We should notice that the former gives the underestimation of the deposition power and the latter does the

overestimation, as shown in Fig. 2.

The total absorbed power evaluated by integrating the profile of Fig. 2 gives $P_{e,total}$ = 0.53 MW, although the rf power delivered from the antenna is P_{net} = 0.9 MW. This discrepancy is reasonably accounted for, because the coupling of the rf power to the core plasma is 80 ~ 100 %, derived from the time derivative of the total stored energy, among which the fraction for the electron heating is calculated to be 60 ~ 80 % with the global wave code, as described later.

III. Theoretical study on the deposition profile

The ICRF wave has been theoretically studied with two different treatments; one is an optical approximantion in the ray-tracing code, and another is a boundary-value treatment in the global wave code. In the ray-tracing code, it is easy to take the complex magnetic geometry into account, and to introduce various kinetic effects, and on the contrary, the tunnelling effect beyond the two-ion hybrid evanescent layer can not be handled. The global wave code are suitable to study the distribution of the rf power to each species, and some kinetic effects such as a mode-conversion to the Ion Bernstein wave and 1st/2nd harmonic cyclotron damping are taken into account. Here with these two different codes, we have analyzed the distribution of the rf power to each species and the deposition profile in electrons.

As for the global wave code, we have employed the ICH code developed by A. Fukuyama *et al.* [6]. The model used in the calculation is a two-dimensional slab geometry (radial mesh along the major radius; N = 200 ~ 400 meshes, and toroidal Fourier mode $k_\phi = n/R_{maj}$, n = ±1 ~ ±32). Figure 3 shows the radial profile of the rf power deposited to each species (electron, hydrogen and deuterium) with its dispersion relation.

Plasma parameters employed in the computer code are as follows; $T_{e,i}(r) = T_{e,i}(0)(1-(r/a)^2)^2$, and $n_e(r) = n_e(0)(1-(r/a)^2)$ with $T_e(0) = 2.0\ keV$, $T_{HD}(0) = 1.0\ keV$ and $n_e(0) = 10^{20}\ m^{-3}$. The fast wave launched at the high-field-side (HFS) antenna is converted to the Ion Bernstein wave around the plasma center, resulting in being absorbed by electrons through the Landau damping. By the tunnelling effect, some part of the fast wave can propagate beyond the two-ion hybrid layer, and is absorbed by hydrogen ($\omega = \Omega_{CH}$) and deuterium ($\omega = 2\Omega_{CD}$) ions. The dominant part of the rf power is absorbed by electrons ($\hat{P}_e > 80$ %) through the Landau damping of the mode-converted IBW, and the remainder is by hydrogen ions ($\hat{P}_H < 20$ %) through the 1st harmonic cyclotron damping of the fast wave. The absorption by deuterium ions through 2nd harmonic cyclotron damping is negligibly small ($\hat{P}_D \sim 1$ %).

To investigate the distribution of the rf power to each species in a wide scope, we have taken the following three cases into account; (a) the high energy ions, (b) the percentage of the hydrogen (i.e., $n_H/(n_H+n_D)$) and (c) non-fully ionized impurity ions. Results are shown in Fig. 4(a)-(c).

The power distribution has been calculated as a function of the effective tail temperature in Fig. 4(a), keeping the density of the high energy tail to be $n_{H,tail}/n_{H,bulk} = 10$ %. When the tail temperature extends up to $T_{H,tail} = 6 \sim 7\ keV$, it is expected that 30 ~ 40 % of the rf power is delivered to hydrogen ions. This result, furthermore, implies that the percentage of the rf power to hydrogen ions increases nonlinearly with the rf power, because the high energy tail is strongly enlarged as the rf power is increased.

It is not so easy to control the amount of hydrogen-minority, because it strongly depends on the wall condition. We usually monitor the ratios of H_α/D_α lines and H/D charge-exchange signals, and estimate to be $n_H/(n_H+n_D) = 10 \sim 20$ %. Figure 4(b) shows the power partition as a function of the hydrogen percentage. We can see that when the

percentage is reduced below 6 %, the rf power couples dominantly with hydrogen ions.

We have considered the power absorption due to impurity ions. The low-Z impurities (e.g., Carbon and Oxygen) are fully ionized around the plasma center, and the 2nd harmonic cyclotron resonance layer is coincident with that of the deuterium ions. Then, it is expected that low-Z impurity ions couple to the fast wave with a similar way of deuterium ($\omega = 2\Omega_{CD}$), and the absorption of the rf power is negligibly small. While, the high-Z impurities (e.g., Titanium and Iron) is not fully ionized in these experimental parameters. The cyclotron resonance layers for non-fully ionized impurities move toward the high-field-side beyond the two-ion hybrid layer. Here we have calculated the power absorption, by introducing a Titanium ion with Z = 20 (i.e., Ti^{20+}), which is existing around the plasma center and is one of the dominant impurities in these experiments. The position of the 2nd harmonic layer for Ti^{20+} ions are pointed out in Fig. 3(a), and Fig. 4(c) shows the power distribution as a function of Ti^{20+} density. It is understood that the mode-converted IBW is absorbed by Ti^{20+}. Even if the density of Ti^{20+} is around 0.03 %, the power delivered to Ti^{20+} ions becomes around 10 %. At the present experiments, the amount of Ti^{20+} ions was, unfortunately, not measured, and it was not so clear in the data of the Doppler profile measured with a crystal spectrometer to identify some evidence for the direct heating of Ti^{20+} ions [16].

We could conclude from these considerations that the rf power consumed incidently to the electron heating is 60 ~ 80 % of the rf power, and the remainder is delivered to hydrogen/impurity ions.

Next, concerning to the deposition profile, it is not appropriate to compare the experimental data with results of the global wave code, because 2-D slab-geometry is employed, as shown in Fig. 3. To examine the deposition profile of the rf power for electrons, we have employed the ray-tracing code [5].

Figure 5(a) shows the profile of the rf power delivered to electrons, where the deposition profiles for various $k_{\parallel}$ values are also presented. Ray trajectories for $k_{\parallel}$ = 3 and 15 m^{-1} are presented in Fig. 5(b). The fast wave launched at the high-field-side is mode-converted into IBW and absorbed by electrons. The calculational results show that the spatial width of the deposition profile is about 5 cm in each $k_{\parallel}$ value. As the $k_{\parallel}$ value becomes larger, the deposition region shifts toward the low-field side (i.e., toward the plasma center in our experimental parameters). The spatial distance of the deposition region for $k_{\parallel}$ = 3 and 15 m^{-1} cases is about 5 cm. Consequently, the deposition profile of mode-converted IBW becomes broader, as shown in Fig. 5(a), while the cyclotron damping of the fast wave is very localized at the resonance layer. This characteristics is qualitatively supported by the results with the global wave code, as shown in Fig. 3.

We can, therefore, say that the relatively broad deposition profile experimentally obtained in Fig. 2 is consistent with the predictions of the ray-tracing and the global wave codes, although the quantitative agreement is not so good.

IV. Electron thermal diffusivity

In ICRF heating experiments, it is not so straightforward to evaluate the electron thermal diffusivity, because the deposition profile of the rf power to electrons is not well understood theoretically. Since we have experimentally determined the deposition profile, as presented in the previous section, the electron thermal diffusivity, χ_e, has been evaluated by using the experimental data.

The equation employed to evaluate the electron thermal diffusivity is given by

$$\chi_e(r) = \frac{1}{4\pi^2 R_0 r n_e(r) \left| \frac{\partial T_e}{\partial r} \right|} \int_0^r (P_{oh} + P_{rf,e} - P_{ei} - P_{rad} - W_e - P_{conv}) dV_p \quad . \qquad 3$$

where P_{oh}, $P_{rf,e}$, P_{ei}, P_{rad} and P_{conv} are powers of the ohmic, the rf to electrons, the equipartition between electrons and ions, the radiation loss and the convection, respectively, and W_e is the derivative of the electron stored energy. In calculating eq.(3), the profile data measured for the electron temperature, the density and the radiation loss are used. The central ion temperature is also measured, its profile being assumed to be the same with the electron one. The ohmic power profile is assumed to be subject to the ohm's law, i.e., $j(r) \propto T_e^{3/2}(r)$, using the total ohmic power of the experimental value.

In Fig. 6, each term in the right hand side of eq.(3) is plotted as a function of the minor radius, and the value of χ_e is also presented. Inside $q < 1$ ($r/a \sim 0.3$) and outside $r/a \sim 0.7$, the values of χ_e have less meaning, because of the sawtooth relaxation and the convection effect, respectively. At the region $0.3 < r/a < 0.7$, the conduction loss is dominant, the other loss channels (P_{ei}, P_{rad} etc.) being insignificant. The value of χ_e is around 0.65 m^2/s at $\bar{n}_e = 9\times10^{19}$ m^{-3}, and shows a broad profile because the density profile is very flat at $r/a < 0.7$ in these experiments. This value is, roughly speaking, in agreement with INTOR/Alcator scaling [20] and DIII-D data [21], where χ_e (m^2/s) = (5 ~ 6.5) x 10^{19} / n_e (m^{-3}), giving $\chi_{e,INTOR} \sim 0.6$ m^2/s, although we could not examine the density dependence of χ_e because the density dynamic range of the density is unfortunately not so wide in our ICRF experiments.

The energy confinement time determined by the electron heat conduction, $\langle\tau_E\rangle$ ($= a^2/(4\chi_e)$), is calculated to be $\langle\tau_E\rangle \sim 20$ ms. The value of $\langle\tau_E\rangle$ is in agreement with the global energy confinement time τ_E ($= W_P/P_{input}$). We could say that the electron heat conduction govern the plasma confinement for almost whole plasma volume, and there exists no good confinement zone at the plasma periphery such an H-mode [22].

V. Conclusions

In ICRF heating experiments the deposition profile in electrons has been derived experimentally, with the decay rate of the electron temperature just after the switch-off of the rf pulse. It is observed in JIPP T-IIU experiments that the deposition profile is relatively broad ($P_{rf,e}(r) = P_{rf,e}(0)(1-(r/a)^2)^k$ with $k = 1.8$), and the rf power deposited inside $q = 1$ surface is not so large ($\hat{P}_{rf}(q<1) = 20 \sim 30$ %) compared with those in JET and PLT ($\hat{P}_{rf}(q<1) = 50 \sim 80$ %). This is caused by the difference of the heating scheme; i.e., the mode-converted IBW heating in JIPP T-IIU and the fast wave heating in JET and PLT. The distribution of the rf power to each species (electrons, hydrogen and deuterium ions) is in good agreement with theoretical predictions calculated with the global wave code. We should notice that even if the amount of non-fully ionized impurity ions (e.g., Ti^{20+}) is around 0.03 %, the rf power of 10 % or more is absorbed by these impurity ions, because the cyclotron resonance layers for non-fully ionized impurity ions lie on the mode-converted IBW at the high-field-side. With the deposition profile obtained experimentally, the electron thermal diffusivity χ_e has been calculated to be $\chi_e \sim 0.65\ m^2/s$ at $\bar{n}_e = 9\times10^{19}\ m^{-3}$, and the resulting confinement time $\langle\tau_E\rangle$ ($= a^2/(4\chi_e)$) is in good agreement with the global energy confinement time τ_E ($= W_P/P_{input}$).

Acknowledgements

The authors would like to thank Dr. A. Fukuyama and Prof. T. Amano for their theoretical support.

a) Present address; National Laboratory for High Energy Physics,
Oho, Tsukuba, Ibaraki 305, Japan

References

[1] J.K. Munro, J.T. Hogan, H.C. Howe, D.E. Arnurius, "A User's Manual for the Oak Ridge Tokamak Transport Code", ORNL/TM-5262 (1977).

[2] R.H. Fowler, J.A. Holmes, J.A. Rome, "NFREYA - A Monte Carlo Beam Deposition Code for Non-circular Tokamak Plasmas", ORNL/TM-6845 (1979).

[3] Hawryluk, R.J., in Physics of Plasmas Close to Thermonuclear Conditions(Proc. Course Varenna, 1979), Rep. EUR-FU-BRU/XII/476/80, CEC, Brussels (1980) 19.

[4] A.H. Kritz, H. Hsuan, R.C. Goldfinger, D.B. Batchelor, in Heating in Toroidal Plasmas, (Proc. 3rd Joint Varenna-Grenoble Int. Sympo., Grenoble, 1982), Vol. 2, CEC, Brussels (1982) 707.

[5] B.D. McVey, Nucl. Fusion, 19, (1979) 461.

[6] A. Fukuyama, S. Nishiyama, K. Itoh, S.-I. Itoh, Nucl. Fusion, 23 (1983) 1005.

[7] K. Itoh, S.-I. Itoh, A. Fukuyama, Nucl. Fusion, 24 (1984) 13.

[8] E.F. Jaeger, D.B. Batchelor, H. Weitzner, J.H. Whealton, Comput. Phys. Commun., 40 (1986) 33.

[9] K. Appert, T. Hellsten, J. Vaclavik, L. Villard, Comput. Phys. Commun., 40 (1986) 73.

[10] T. Hellsten, L. Villard, Nucl. Fusion, 28 (1988) 285.

[11] D.J. Gambier, D.V. Bartlett, M. Bures, D.J. Campbell, G.A. Cotrell, et al., in Controlled Fusion and Plasma Heating (Proc. 12th Europ. Conf. , Budapest, 1985), Vol.9F part II, European Physical Society (1985) 152.

[12] JET Team, in Plasma Physics and Controlled Nuclear Fusion Research 1986 (Proc. 11th Int. Conf., Kyoto, 1986) Vol.I, IAEA, Vienna (1987) 449.

[13] T. Watari, K. Ohkubo, R. Akiyama, R. Ando, D. Eckhartt, et al., ibid., 495.

[14] Y. Ogawa, K. Masai, T. Watari, R. Akiyama, R. Ando, et al., "High Power ICRF Heating Experiments on the JIPP T-IIU Tokamak",

IPPJ-903 (1989).

[15] K. Kawahata, K. Sakai, R. Ando, S. Ohara, J. Fujita, Jpn. J. Appl. Phys., 27, (1988) 2349.

[16] S. Morita, Y. Ogawa, T. Watari, R. Akiyama, K. Kadota, Y. Kawasumi, T. Ozaki, M. Sasao, K. Sato, in Controlled Fusion and Plasma Heating (Proc. 14th Europ. Conf. , Madrid, 1987), Vol.III, European Physical Society (1987) 874.

[17] I. Ogawa, K. Kawahata, Y. Ogawa, T. Watari, N. Noda, K. Masai, E. Kako, S. Tanahashi, K. Toi, J. Fujita, J. Phys. Soc. of Japan, 56, (1987) 535.

[18] J. Jacquinot, R.J. Anderson, J. Arbez, D. Bartlett, B. Beaumont, et al., Plasma Physics and Controlled Fusion, 28 (1986) 1.

[19] J. Hosea, R. Bell, M. Bitter, A. Cavallo, S. Cohen, et al., in Controlled Fusion and Plasma Heating (Proc. 12th Europ. Conf. , Budapest, 1985), Vol.9F part II, European Physical Society (1985) 120.

[20] INTOR Group, Report of Int. Tokamak Reactor Workshop, Phase one, Vienna, (1982)

[21] M. Kasai, M. Nagami, M. Otsuka, H. Aikawa, A. Kitsunezaki, *et al.*, Nucl. Fusion, 25 (1985) 1437.

[22] F. Wagner, G. Becker, K. Behringer, D. Campbell, A. Eberhagen, *et al.*, Phys. Rev. Lett., 49 (1982) 1408.

Figure Captions

Fig. 1 Time evolutions of the electron temperature at different major radii measured with a grating polychromator for ECE measurement, where P_{rf} = 0.9 *MW*.

Fig. 2 Deposition profile of the rf power to electrons derived from the decay rate of the electron temperature just after the switch-off of the rf power. These data are fitted to the form of $P_{rf,e}(r) = P_{rf,e}(0)(1-(r/a)^2)^k$ with $P_{rf,e}(0)$ = 1.57 MW/m^3 and k = 1.8. Virtual deposition powers due to the effects of the high energy ion tail $P_{e,tail}$ and the movement of the plasma column $P_{e,move}$ are also presented.

Fig. 3 (a) The dispersion relation and (b) the power absorption profiles for each species, calculated with the 2-D (radial and toroidal) global wave code, where the fast wave is launched at the high-field-side (HFS) antenna with the finite width (9.5 cm) in the toroidal direction. S_X denotes the energy flux normalized with unity at the plasma boundary. The parameters employed are that $T_{e,i}(r) = T_{e,i}(0)(1-(r/a)^2)^2$, and $n_e(r) = n_e(0)(1-(r/a)^2)$ with $T_e(0)$ = 2.0 *keV*, $T_{HD}(0)$ = 1.0 *keV*, $n_e(0) = 10^{20}$ m^{-3}, and $n_H/(n_H+n_D)$ = 10 %. The locations of $\omega = \Omega_{CH}$ and $\omega = 2\Omega_{CTi^{20+}}$ are also pointed.

Fig. 4 Power distributions calculated with the global wave code for various cases.

(a) High energy tail of hydrogen ions is taken into account, where $n_{H,tail}/n_{H,bulk}$ = 0.1, and other parameters are the same with those of Fig. 3.

(b) A percentage of hydrogen to deuterium is changed, keeping the total density ($n_H + n_D$) constant.

(c) Partially-ionized impurity ion (i.e., Ti^{20+}) is considered, where the mass of Titanium impurity is taken to be

A = 48. The location of the 2nd harmonics cyclotron resonance for Ti^{20+} is shown in Fig. 3.

Fig. 5 (a) Deposition profile in electrons calculated with the ray-tracing code, where $n_H/(n_D+n_H)$ = 0.15, $T_e(0)$ = 2.0 keV, $T_i(0)$ = 1.0 keV and $n_e(0)$ = 1.0×10^{20} m^{-3}. The deposition profiles for various $k_{\parallel}$ values are also presented.
(b) Ray trajectories for $k_{\parallel}$ = 3 and 15 m^{-1}, respectively.

Fig. 6 Local power balance derived from the experimental data and the electron thermal diffusivitv χ_e as a function of the minor radius (r/a), where inside q < 1 (r/a ~ 0.3) and outside r/a ~ 0.7 the values of χ_e have less meaning, because of the sawtooth relaxation and the convection effect, respectively.

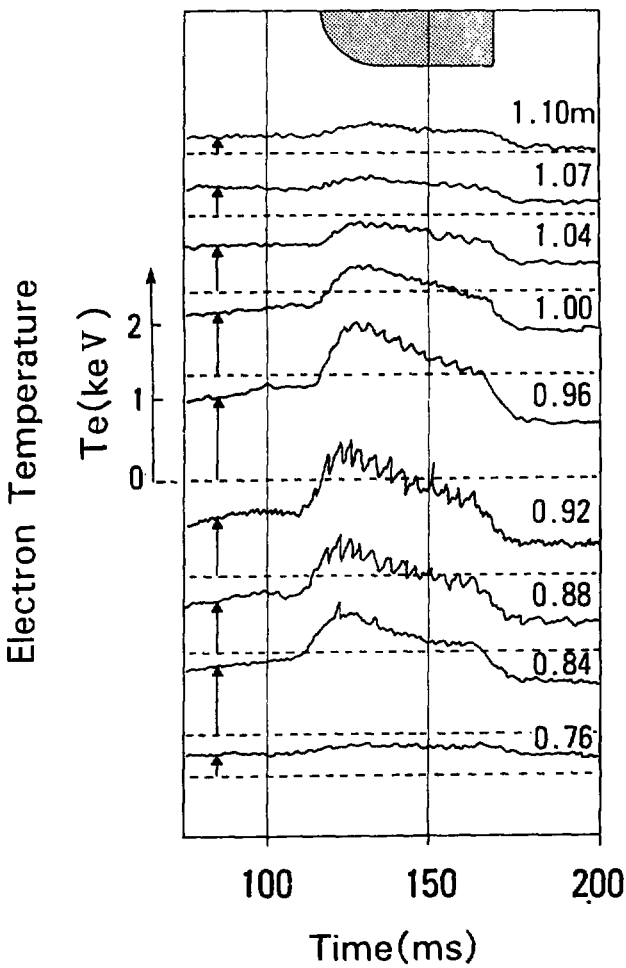
Electron Temperature
Te(keV)
2
1
0
1.10m
1.07
1.04
1.00
0.96
0.92
0.88
0.84
0.76
100
150
200
Time(ms)

Fig. 1

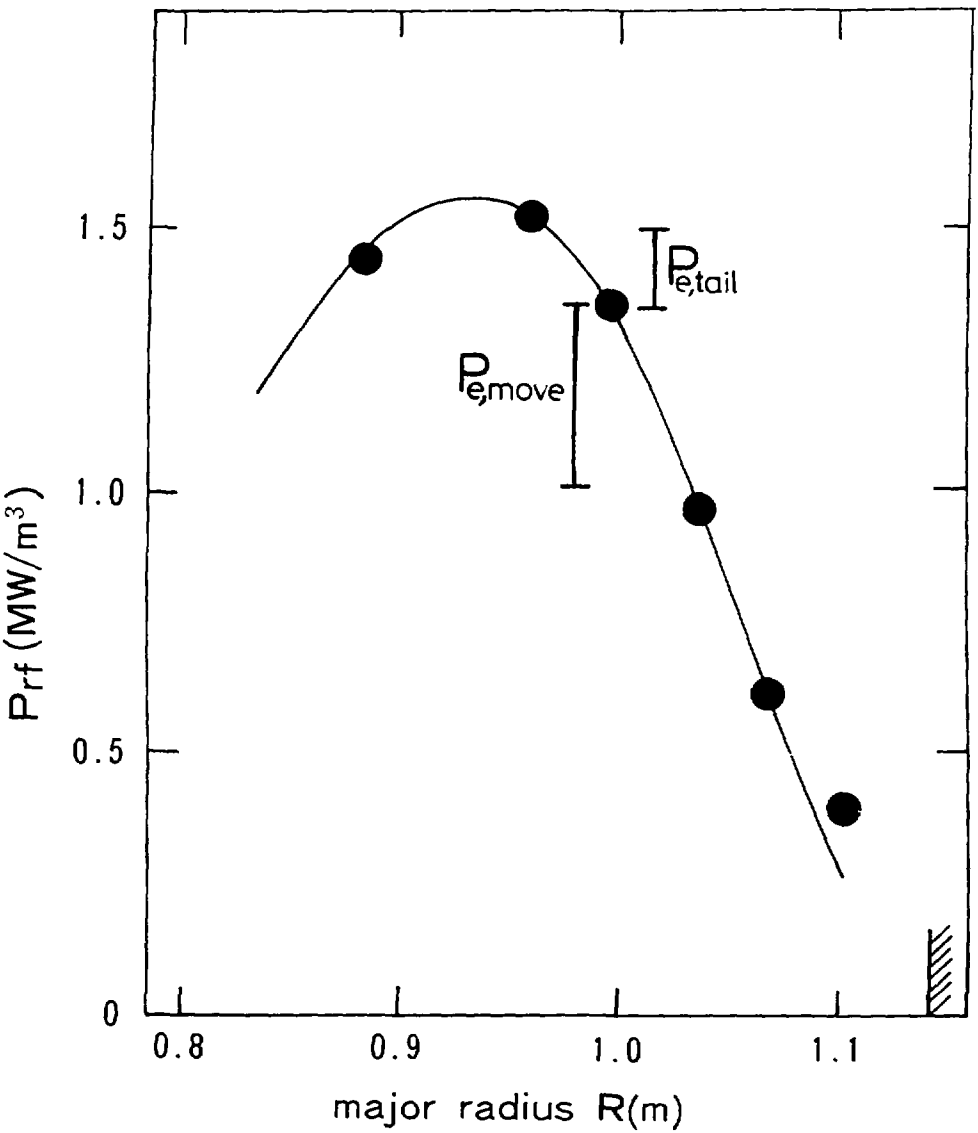

Fig. 2

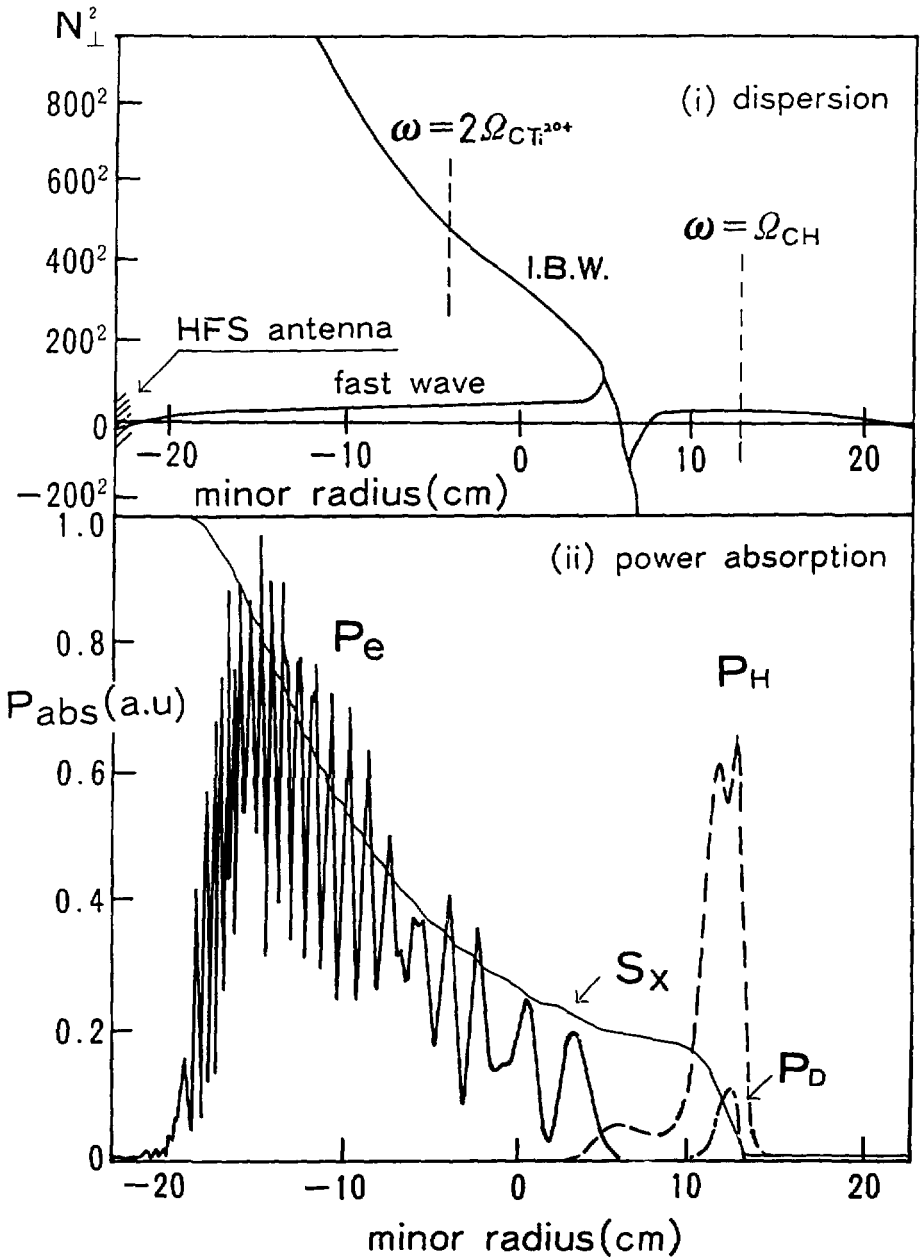
$N_\perp^2$
800^2
600^2
400^2
200^2
0
-200^2
(i) dispersion
$\omega = 2\Omega_{CTi^{20+}}$
$\omega = \Omega_{CH}$
I.B.W.
HFS antenna
fast wave
−20
−10
0
10
20
minor radius(cm)
1.0
0.8
0.6
0.4
0.2
0
P_{abs}(a.u)
(ii) power absorption
P_e
P_H
S_X
P_D
−20
−10
0
10
20
minor radius(cm)

Fig.3

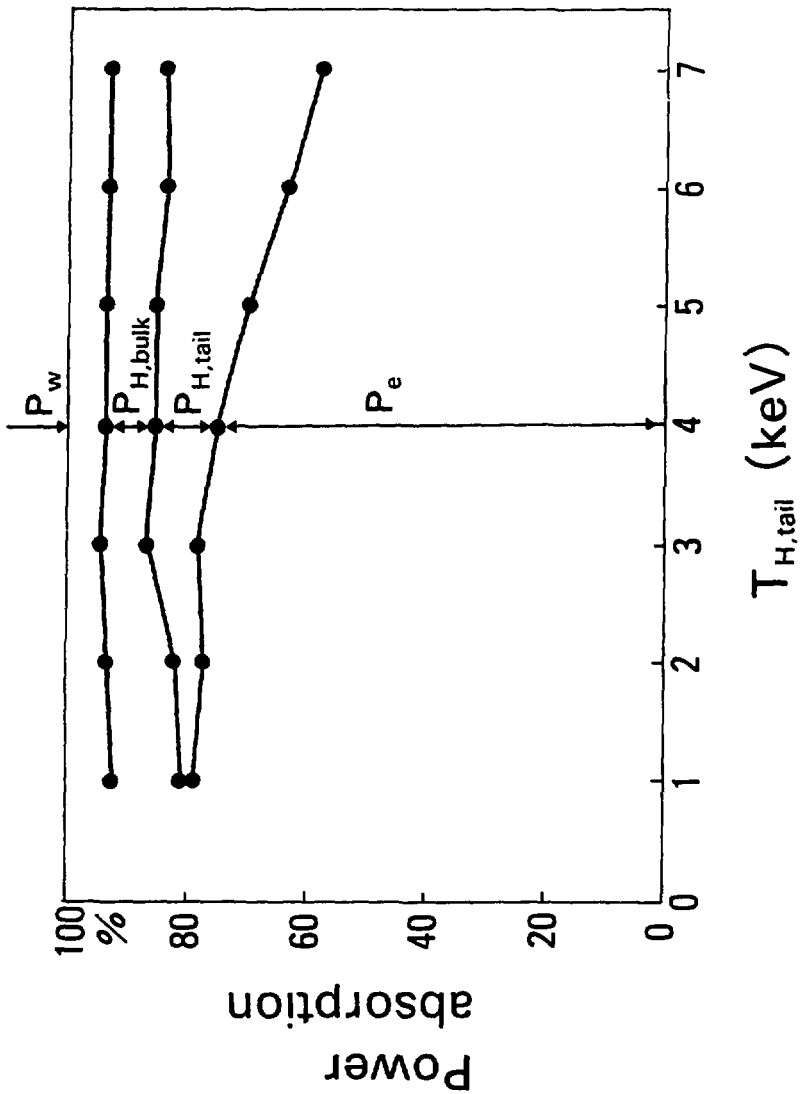
Power absorption
100 %
80
60
40
20
0
0
1
2
3
4
5
6
7
$T_{H,tail}$ (keV)
P_w
$P_{H,bulk}$
$P_{H,tail}$
P_e

Fig. 4 (a)

Fig. 4(b)

Power
absorption
0
20
40
60
80
100
%
0.001
0.01
0.1
$n(T_i^{20+})/n_e$ (%)
P_e
$P_{imp.}$
P_H
P_W

Fig. 4 (c)

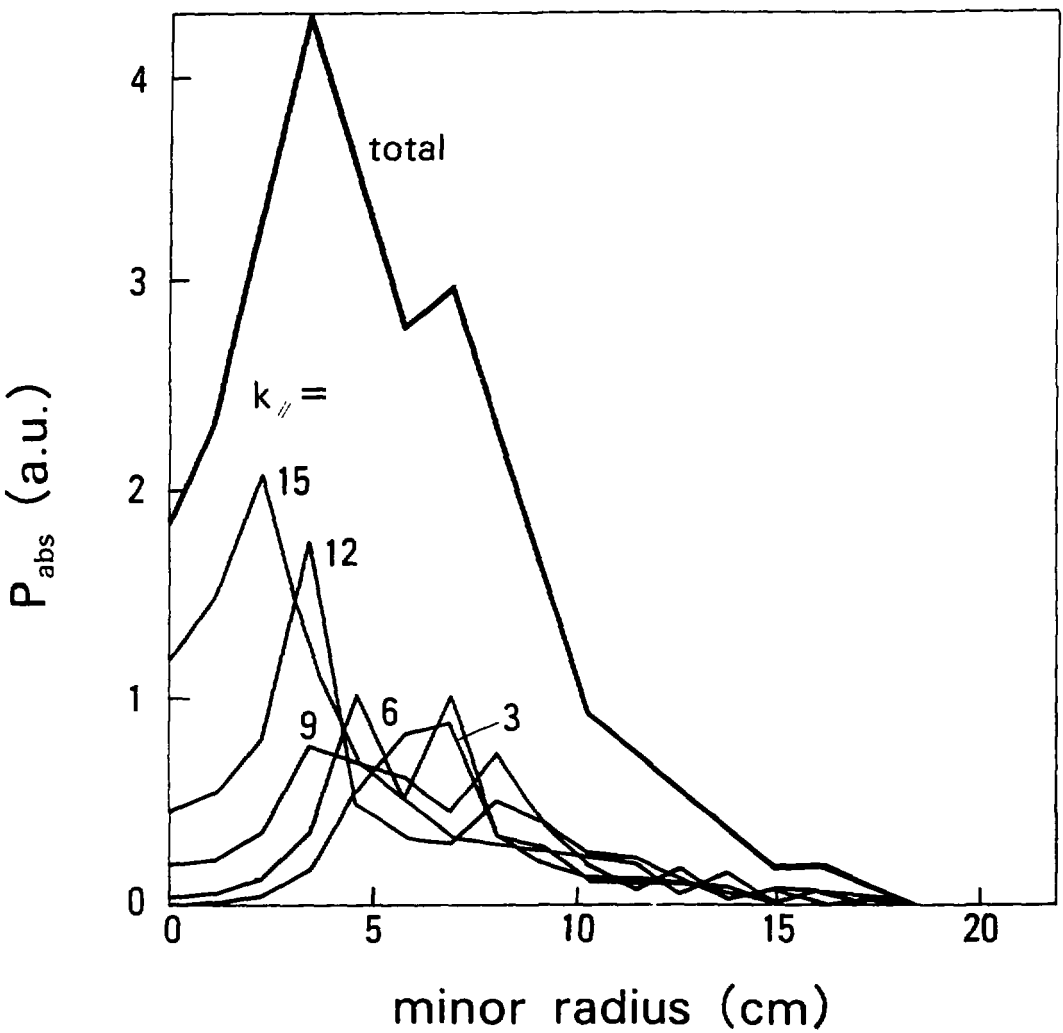

Fig.5(a)

Fig.5(b)

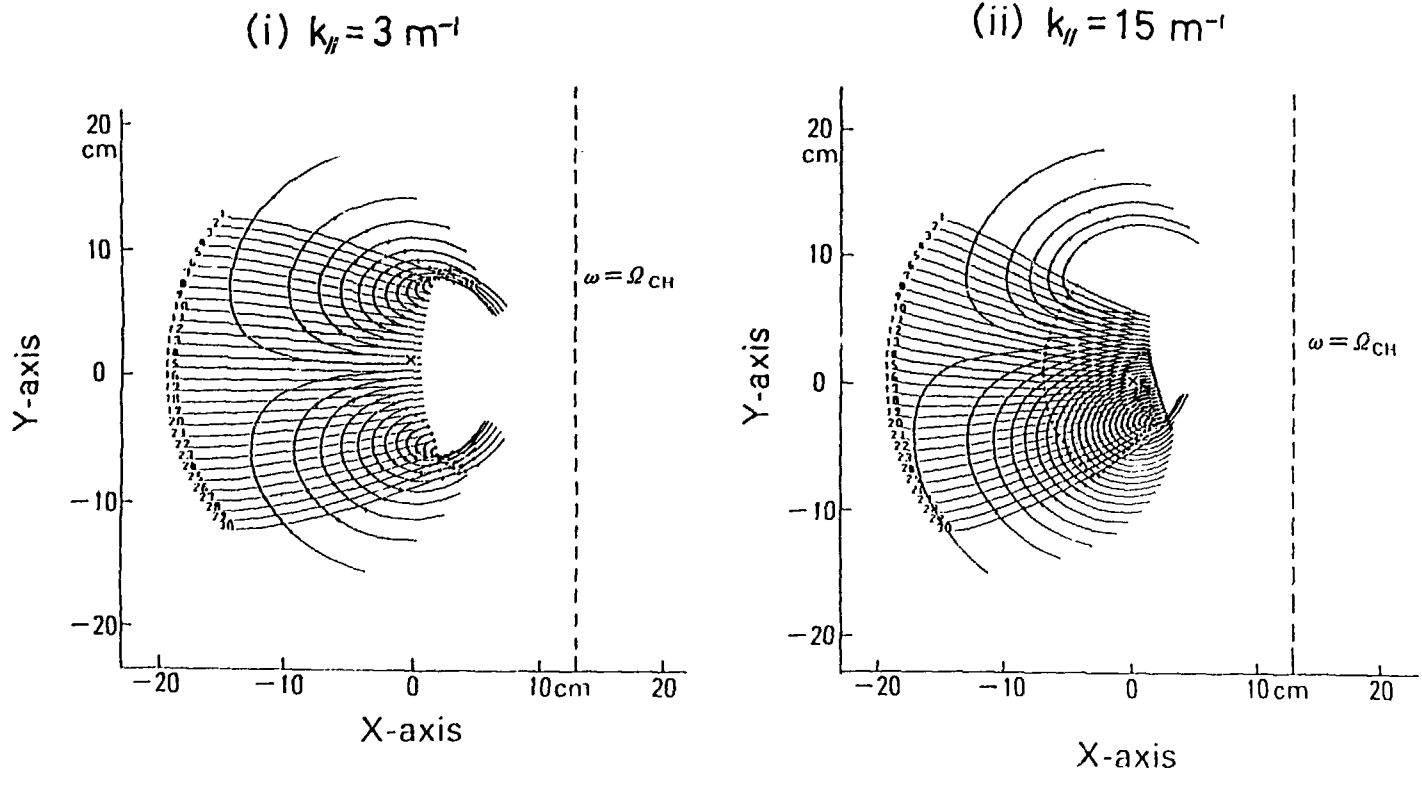
(i) $k_{//} = 3\ m^{-1}$
(ii) $k_{//} = 15\ m^{-1}$
20 cm
10
0
−10
−20
Y-axis
−20
−10
0
10cm
20
X-axis
$\omega = \Omega_{CH}$

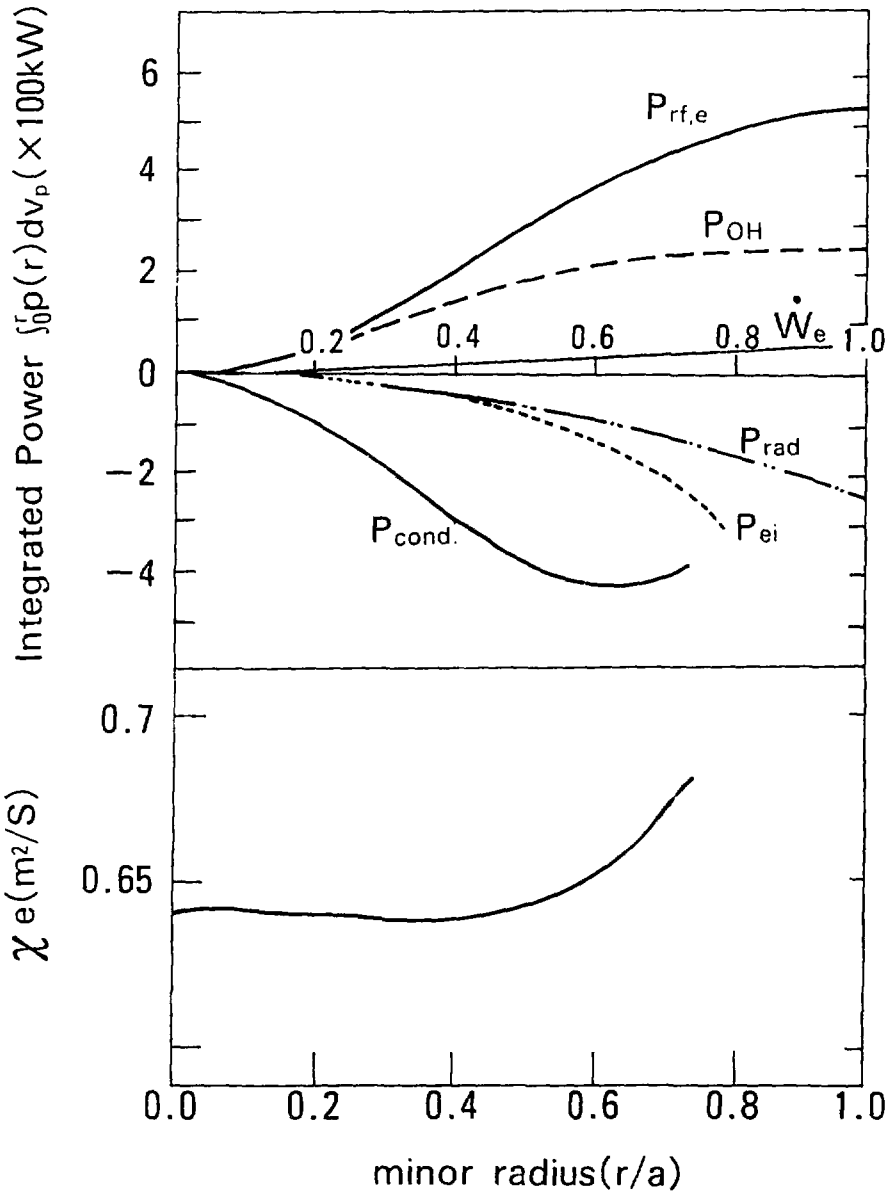
Integrated Power $\int_0^r p(r)dv_p$ (×100kW)
6
4
2
0
−2
−4
$P_{rf,e}$
P_{OH}
0.2
0.4
0.6
0.8
$\dot{W}_e$
1.0
P_{rad}
P_{ei}
$P_{cond.}$
χ_e(m²/S)
0.7
0.65
0.0
0.2
0.4
0.6
0.8
1.0
minor radius(r/a)

Fig. 6